

Interplay of structure and charge order revealed by quantum oscillations in thin films of $\text{Pr}_2\text{CuO}_{4\pm\delta}$

Nicholas P. Breznay ^{*}, Ian M. Hayes, Nityan L. Nair, Toni Helm, and James G. Analytis[†]
Materials Science Division, Lawrence Berkeley National Laboratory, Berkeley, California 94720, USA
and Department of Physics, University of California, Berkeley, Berkeley, California 94720, USA

Ross D. McDonald and Zengwei Zhu
National High Magnetic Field Laboratory, Los Alamos National Laboratory, Los Alamos, New Mexico 87545, USA

Yoshiharu Krockenberger, Hiroshi Irie, and Hideki Yamamoto
NTT Basic Research Laboratories, NTT Corporation, 3-1 Morinosato-Wakamiya, Atsugi, Kanagawa 243-0198, Japan

K. A. Modic
Max-Planck-Institute for Chemical Physics of Solids, Dresden 01187, Germany
and National High Magnetic Field Laboratory, Los Alamos National Laboratory, Los Alamos, New Mexico 87545, USA

Alex Frano
Advanced Light Source, Lawrence Berkeley National Laboratory, Berkeley, California 94720, USA
and Department of Physics, University of California, Berkeley, Berkeley, California 94720, USA

Padraic Shafer and Elke Arenholz
Advanced Light Source, Lawrence Berkeley National Laboratory, Berkeley, California 94720, USA



(Received 11 January 2017; revised manuscript received 28 October 2019; published 6 December 2019)

The discovery of quantum oscillations in hole- and electron-doped cuprate families has underscored the importance of the Fermi surface in cuprate superconductivity. While the observed quantum oscillations in both families have revealed the presence of reconstructed Fermi surfaces, there remains an important distinction between the two. In hole-doped cuprates the oscillations are thought to arise from the effects of a charge density wave, while in the electron-doped cuprates it is thought that these oscillations occur from an antiferromagnetically reconstructed Fermi surface, despite the fact that the oscillations are observed in overdoped compounds, far from the putative antiferromagnetic critical point. In this work we study thin films of $\text{Pr}_2\text{CuO}_{4\pm\delta}$, whose apparent doping can be finely tuned by annealing, allowing studies of quantum oscillations in samples straddling the critical point. We show that even though there is a mass enhancement of the quasiparticles, there are only small changes to the Fermi surface itself, suggesting that charge order is a more likely origin, with electronic correlations that are strongly dependent on the structural parameters.

DOI: [10.1103/PhysRevB.100.235111](https://doi.org/10.1103/PhysRevB.100.235111)

I. INTRODUCTION

The identity of the quantum ordered states in the phase diagram of the cuprate superconductors is arguably the most important determination required to understand the superconductivity itself. In the last decade, scattering and quantum oscillatory measurements have revealed the existence of previously unknown phases, most notably the presence of a charge density wave which appears to compete with superconductivity to set the ground state. The electron-doped cuprate $\text{Pr}_{2-x}\text{Ce}_x\text{CuO}_4$ has a temperature-doping phase diagram that can be divided into underdoped and overdoped regions, with a dome of superconductivity that straddles the two (Fig. 1). The underdoped (UD) region is characterized by a number

of phase instabilities and low carrier densities roughly equal to the number of dopants (x per Cu). The overdoped (OD) region is characterized by more conventional metallic behavior and a high carrier density n (approximately one hole per Cu). The dominant phase instability in underdoped T' materials is (π, π) antiferromagnetic order, as observed in $\text{Nd}_{2-x}\text{Ce}_x\text{CuO}_4$ [1–3]; this order is suppressed by doping, leading to a putative quantum critical point (QCP) whose presence may serve to enhance the superconducting critical temperature T_c .

The quantum oscillations measured in hole-doped cuprates are now thought to arise from a charge density wave (CDW), an explanation ultimately confirmed by scattering measurements which even showed that the application of a magnetic field enhances the CDW to the detriment of the superconductivity [4,5]. Quantum oscillations (QOs) in the electron-doped cuprate $\text{Nd}_{2-x}\text{Ce}_x\text{CuO}_4$ have had a very different interpretation, thought to arise from a (π, π) antiferromagnetically

^{*}Corresponding author: nbreznay@hmc.edu

[†]Corresponding author: analytis@berkeley.edu

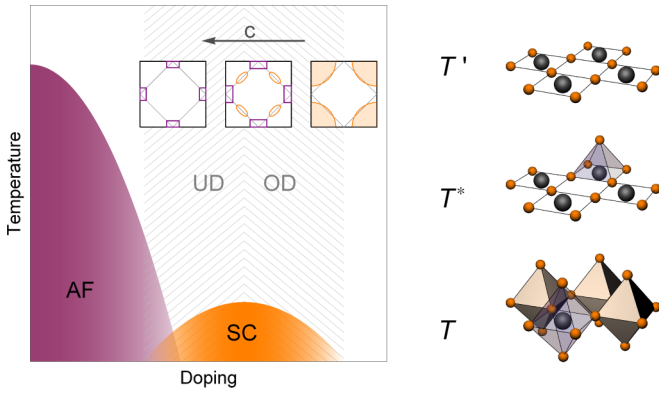


FIG. 1. Crystal structure and phase diagram of $\text{Pr}_2\text{CuO}_{4\pm\delta}$. Left: Schematic phase diagram of the conventional picture of the electron-doped cuprates which does not include charge order instabilities; inset shows possible evolution of the Fermi surface with doping. Right: The checkerboard in-plane CuO_2 unit cell of T' $\text{Pr}_2\text{CuO}_{4\pm\delta}$, a pyramidal Cu coordination (T^*) formed by an oxygen defect, and the octahedrally coordinated (T) structure of, e.g., hole-doped $\text{La}_{2-x}\text{Sr}_x\text{CuO}_4$.

reconstructed Fermi surface [6]. At high field magnetic breakdown orbits have also been observed, with QO frequencies corresponding to an unreconstructed Fermi surface. However, this interpretation presents two challenges. First, the quantum oscillations are observed at dopings far from the antiferromagnetic (AFM) critical point. In fact, to our knowledge, QOs on the AFM side of the phase diagram have never been observed in the electron-doped cuprates. Second, if magnetic breakdown is observable, then two frequencies should also be observable from the reconstructed Fermi surface (one electronlike and another holelike pocket, commonly observed in electron-doped compounds [7]), but only one has ever been seen experimentally. Ideally, QO studies in samples approaching the AFM critical point from either side can help reconcile these discrepancies, but it has proven difficult to maintain high electronic mobilities at these compositions of $\text{Nd}_{2-x}\text{Ce}_x\text{CuO}_4$.

Recent resonant x-ray scattering (RXS) measurements of electron-doped $\text{Nd}_{2-x}\text{Ce}_x\text{CuO}_4$ and its cousins present another possible interpretation of the QOs, the existence of a CDW [8–10]. At compositions spanning the AFM critical point a new translational symmetry is observed to onset corresponding to an incommensurate CDW. The in-plane periodicity of the CDW in $\text{Nd}_{2-x}\text{Ce}_x\text{CuO}_4$ is observed to smoothly evolve from $q \sim (0.17, 0)$ to $q \sim (0.28, 0)$ r.l.u. (reciprocal lattice units) as the composition changes from overdoped to underdoped, with no apparent anomaly at the AFM quantum critical point. Note that this is similar to what is observed in the hole-doped cuprates, which show similar CDW wave vectors.

In this work we study thin films of the electron-doped cuprate $\text{Pr}_2\text{CuO}_{4\pm\delta}$. Normally, this system is tuned across its phase diagram by changing the Ce composition x of $\text{Pr}_{2-x}\text{Ce}_x\text{CuO}_4$, but the Ce doping introduces disorder which tends to decrease mobility. Though it is possible to see quantum oscillations in doped thin films, as we recently showed [11], in this study we improve mobilities further by focusing

on annealed $\text{Pr}_2\text{CuO}_{4\pm\delta}$, relying on oxygen stoichiometry to change the doping while keeping mobilities high. As a consequence, we are able to observe QOs across the putative AFM critical point, which has not thus far been possible in bulk crystals. We observe that while the effective mass associated with the QOs appears strongly enhanced close to the QCP, the QO frequency itself changes very weakly and with an opposite trend to what is observed in $\text{Nd}_{2-x}\text{Ce}_x\text{CuO}_4$. This suggests that while the QOs are affected by strong electronic correlations near the QCP, the broken translational symmetry leading to the reconstruction is altered only weakly. Such weak evolution is not what is expected of an AFM reconstruction, but is what is observed for the CDW in the related compound $\text{Nd}_{2-x}\text{Ce}_x\text{CuO}_4$. In order to make this argument we demonstrate that (i) the annealed systems are indistinguishable from their doped counterparts (except in having higher mobility), (ii) the QCP can be identified from the Hall number, and (iii) QOs can be seen at all compositions.

Superconductivity in the cuprates is intricately linked to CuO_2 planes; in Pr_2CuO_4 the T' crystal structure (shown in Fig. 1) is composed of oxygen-coordinated Cu atoms that form prototypical CuO_2 planes. The two-dimensional (2D) electronic band structure features a large holelike cylinder centered at $(ak_x, ak_y) = (\pi, \pi)$ (Fig. 1, inset). Changes to the oxygen stoichiometry affect both the carrier concentration of the material and the local copper coordination from square-planar to pyramidal (T^*) or octahedral (T), as illustrated in Fig. 1. The interlayer lattice constant c is found to track, and hence can be used as a measure of, an effective doping x (discussed further below). In this paper we focus on three samples clustered around optimal T_c in the superconducting part of the phase diagram (hatched region in Fig. 1), by following the evolution of the ground state Fermi surface (FS).

The prevailing picture of Ce and oxygen doping (see Ref. [3] for a thorough review) is that Ce is an electron donor, and oxygen a hole donor. Most studies of single crystals and thin films report a combination of annealing and chemical doping to induce superconductivity, complicating a robust accounting of the number of doped carriers in the T' materials [12–15]. However, there are several consistent trends. As the number of charge carriers increases, the antiferromagnetic insulating state is suppressed, giving rise to superconductivity. Maximal $T_c \sim 25$ K is achieved near “optimal” doping of $x \sim 0.15$, where the materials undergo a crossover in the low-field Hall effect from measuring $n \sim x$ to $n \sim 1 \pm x$ [12,16]. Near this crossover, the effective mass is strongly enhanced, implying the presence of strong interelectronic correlations near a possible QCP [17]. However, changing the oxygen stoichiometry δ is known to cause multiple effects including stabilization of antiferromagnetic order, addition of charge carriers, and tuning of disorder [13,16,18]. While precisely tracking δ remains an outstanding challenge [19,20], as argued below, our samples access a crucial part of the cuprate phase diagram near the putative QCP, with minimal disorder that allows for direct study of their FS.

II. METHODS

$\text{Pr}_2\text{CuO}_{4\pm\delta}$ films studied in this work are 100 nm thick, grown via molecular beam epitaxy on (001) SrTiO_3

TABLE I. Sample characterization parameters. Data shown for three $\text{Pr}_2\text{CuO}_{4\pm\delta}$ samples measured in this work, as well as (for reference) Ce-doped films synthesized using similar conditions. Parameters include interlayer lattice parameter c , low-temperature (30 K) resistivity $\rho_{30\text{ K}}$, residual resistivity ratio (RRR), superconducting transition temperature T_c , and ℓ_{tr} the transport mean free path (see Supplemental Material). Results from the quantum oscillation analysis are separated at right: ℓ_D the mean free path extracted using the Dingle temperature T_D , quantum oscillation frequency F , and the quasiparticle effective mass m^* .

Sample	Composition	c (Å)	$\rho_{30\text{ K}}$ ($\mu\Omega\text{ cm}$)	RRR	T_c (K)	ℓ_{tr} (nm)	ℓ_D (nm)	T_D (K)	F (T)	m^* (m_e)
S1	$\text{Pr}_2\text{CuO}_{4\pm\delta}$	12.201	28	9.2	25.0	23	4.5	23	309 ± 15	1.3 ± 0.2
S2	$\text{Pr}_2\text{CuO}_{4\pm\delta}$	12.196	61	9.6	25.7	17	3.4	41	316 ± 15	0.55 ± 0.1
S3	$\text{Pr}_2\text{CuO}_{4\pm\delta}$	12.191	27	7.3	20.5	13	4.1	28	349 ± 15	0.70 ± 0.15
Ref. [11]	$\text{Pr}_{1.86}\text{Ce}_{0.14}\text{CuO}_{4\pm\delta}$	12.148	15	10.2	22	6.7	8.2	44	255	0.43

substrates. Aside from small changes in the postgrowth annealing conditions that all follow the two-step annealing process [21], the films are prepared identically; the only structural difference is variation in the c -axis lattice parameter (see Table I). Further details of the synthesis, annealing, and extensive structural characterization of the films are discussed elsewhere [21]. The variation of the lattice parameter almost certainly is caused by variation in oxygen stoichiometry $\pm\delta$. In complex transition metal oxides like the cuprates, oxygen is the constituent element with the smallest mass and the largest filling factor per unit cell volume. Consequently, it seems chemically likely that it is the most mobile element and agitated well before other constituent elements under an annealing process. While several sophisticated experiments have been performed in the past to trace this intricate behavior during the annealing process, e.g., neutron scattering [22,23]

or Mössbauer spectroscopy [24], such tools are inaccessible for the synthesis of superconducting thin films. While we believe annealing is the primary tuning parameter changing the c -axis lattice constant, determining a bijective relationship between annealing to fine gradations in structure remains challenging. Nevertheless, our conclusions are not contingent on this, but rather on systematic changes in the magnetotransport response of our samples as a function of the c -axis lattice constant, both of which can be experimentally determined.

Films were patterned into Hall-bar geometry devices [see Fig. 2(a), inset] for in- ab -plane (ρ_{xx}) and Hall (ρ_{xy}) resistivity measurements using four-point low-frequency techniques at temperatures to 0.3 K with DC magnetic fields to 16 T, and pulsed magnetic fields to 92 T, applied perpendicular to the ab plane. Several Hall bar devices were fabricated and measured from each film and showed identical behavior; data shown

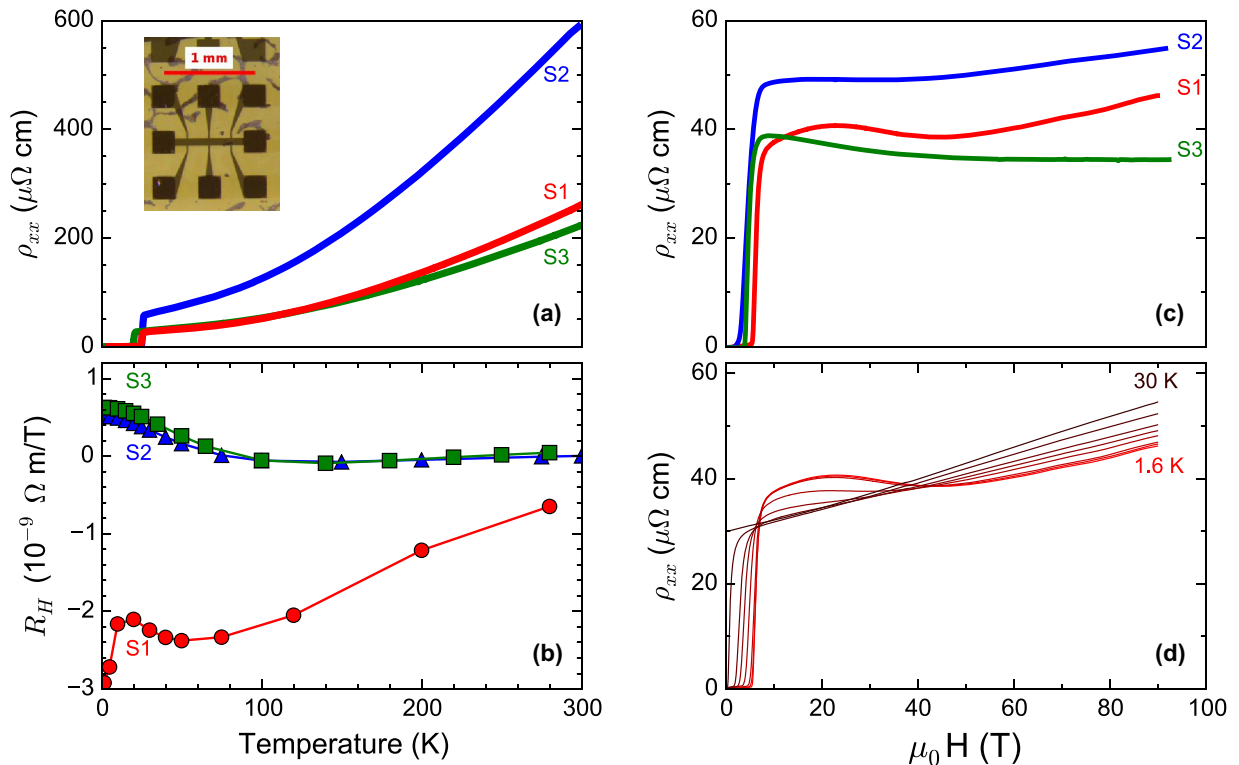


FIG. 2. Transport properties of Pr_2CuO_4 films. (a) Resistivity ρ_{xx} versus temperature for three samples. Inset: optical image of a thin-film Hall bar device; the scale bar is 1 mm. (b) Temperature-dependent Hall coefficient R_H evaluated at $\mu_0 H = 15$ T for all samples. (c) Magnetoresistance measured to 92 T for three samples at $T \approx 2$ K, and as a function of temperature (d) for sample S1.

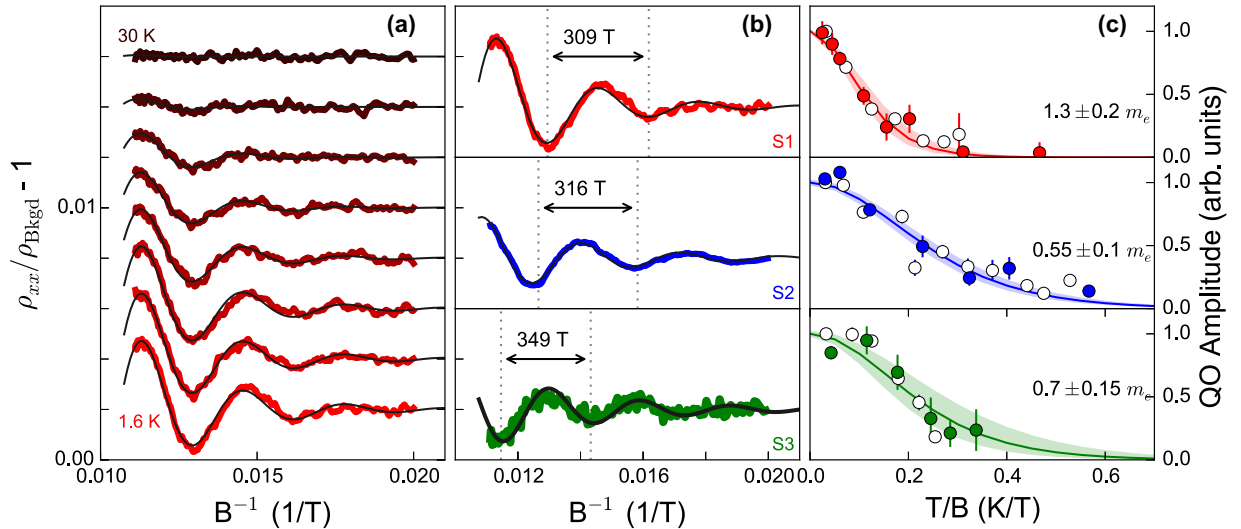


FIG. 3. Magnetic quantum oscillations in $\text{Pr}_2\text{CuO}_{4\pm\delta}$. (a) Background-subtracted resistivity versus inverse field for sample S1 at temperatures between 30 and 1.5 K, along with fits to the Lifshitz-Kosevich formula (see text). (b) Comparison of base temperature data for three samples, along with a single period. (c) Oscillation amplitude decay with T/B for all three samples, yielding the effective mass m^* . Open (filled) circles are FFT (Lifshitz-Kosevich fit) amplitudes.

below are from devices measured to the highest fields available. Modest differences in absolute resistivities reflect gradual improvement in the sample synthesis between different batches of samples; within a given batch, the resistivity changes monotonically. We find no evidence of inhomogeneity in film materials characterization or our transport studies; additional discussions of film characterization data are presented in the Supplemental Material [25]. XRS experiments were performed at Beamline 4.0.2 of the Advanced Light Source. Experiments were conducted between 300 and 15 K under high vacuum ($<10^{-9}$ Torr). Samples were oriented *in situ* using Bragg reflections. All measurements were conducted at the Cu L_3 absorption edge with incoming polarization perpendicular to the scattering plane (σ). Momentum-space scans were obtained by rocking the sample angle at a fixed detector position.

III. RESULTS

Figure 2(a) shows the temperature-dependent resistivity of three Pr_2CuO_4 samples (S1, S2, and S3); the superconducting transition temperature is 20, 25, and 24.5 K for samples S1, S2, and S3, respectively. (Transport data are summarized in Table I.) The temperature dependence of the Hall coefficient R_H is plotted in Fig. 2(b); each trace can be mapped to those seen in Ce-doped $\text{Pr}_{2-x}\text{Ce}_x\text{CuO}_4$ and $\text{Nd}_{2-x}\text{Ce}_x\text{CuO}_4$ [12,17,26]; we associate S1 with $x = 0.13$, S2 with $x = 0.14$, and S3 with $x = 0.17$. In Fig. 2(c), we plot the low-temperature (~ 2 K) magnetoresistance (MR) up to 92 T for each sample; the origin of the hump-shaped feature in the MR and the peculiar sign changing Hall effect [Fig. 2(b)] is a matter of some debate, but has been linked to residual magnetism in $\text{Pr}_{2-x}\text{Ce}_x\text{CuO}_4$ [27]. After crossing through the “hump,” the MR shows Shubnikov–de Haas quantum oscillations in the raw MR traces for all three sam-

ples; at elevated temperatures the oscillations are suppressed [Fig. 2(d)].

In metals, the electronic states are quantized in the presence of a magnetic field B . For sufficiently clean metals the density of states (DOS) becomes an oscillatory function of B and quantities sensitive to the DOS such as conductivity exhibit quantum oscillations (QOs) periodic in B^{-1} . QOs are often difficult to resolve in complex materials (such as transition metal oxides) due to disorder effects, requiring ultrapure systems. As a result, QOs have only been observed in a small group of single-crystal cuprates with a T' structure, $\text{Nd}_{2-x}\text{Ce}_x\text{CuO}_4$ (NCCO) [6] and $\text{Pr}_{2-x}\text{Ce}_x\text{CuO}_4$ [11,28].

We subtract a smoothly varying low-order polynomial from the data shown in Fig. 2 to obtain the relative change in resistivity shown in Fig. 3(a) for sample S1. For such a low frequency of oscillations, there is some sensitivity of subsequent analyses to the choice of background subtraction procedure; results described below are quoted with uncertainties that reflect this sensitivity (details are described in the Supplemental Material). Figure 3(a) shows the low-temperature magnetoresistance for sample S1 plotted versus inverse magnetic field, showing oscillations with an approximate period of 0.003 T^{-1} . The data are well described by the Lifshitz-Kosevich (LK) formula for the oscillating component of the magnetoresistance $\Delta R(B)$ of a quasi-2D FS:

$$\Delta R(B) \propto R_0 R_D R_T \cos(2\pi F/B), \quad (1)$$

where R_0 is an overall amplitude, $R_D = e^{-\pi/\omega_c\tau_D}$ is the Dingle factor, $R_T = \left(\frac{2\pi^2 k_B T/\hbar\omega_c}{\sinh(2\pi^2 k_B T/\hbar\omega_c)}\right)$ is the thermal damping factor, F is the quantum oscillation frequency, $\omega_c \equiv eB/m^*$ is the cyclotron frequency, and m^* is the quasiparticle effective mass [29].

To precisely analyze the quantum oscillatory data, we fit the entire dataset using the LK expression [Eq. (1)] and fixed parameters (such as F). Analysis of the background-

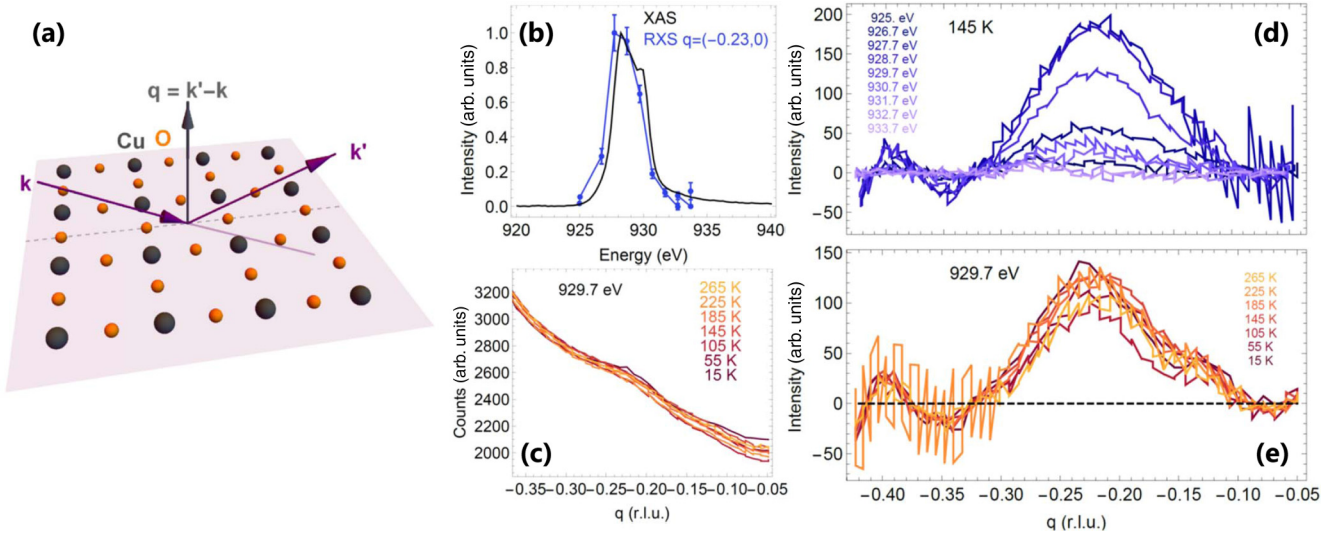


FIG. 4. Resonant x-ray scattering data in $\text{Pr}_2\text{CuO}_{4\pm\delta}$ film S1. (a) Schematic of scattering geometry; k and k' are the incoming and outgoing photon wave vectors, and q is the momentum transfer. (b) Comparison of x-ray absorption spectrum (XAS) intensity and RXS data at fixed q . (c) Temperature dependence of q -resolved intensity about $q = (-0.23, 0)$ r.l.u. (d) RXS scans after subtraction of a smoothly varying background for different incident photon energies. (e) Temperature dependence of charge order peak.

subtracted QO data [shown in Fig. 3(a)] also yields the cyclotron effective mass m^* and the scattering time τ_D . (Additional quantum oscillation data and analyses are shown for samples S2 and S3 in the Supplemental Material.) The orbitally averaged mean free path $l_D = \tau_D \frac{\hbar}{m^*} \sqrt{\frac{F}{\pi}} \approx 4$ nm is smaller than the transport mean free path $\ell_{tr} \approx 20$ nm for all samples; this is as expected since quantum oscillations are sensitive to both small and large angle scattering events. Sample mobilities $\mu_D = \tau_D e / m^* \sim 0.01$ T $^{-1}$.

While F values are comparable to those observed in single-crystal electron-doped materials, and so likely originate from the same FS, they vary systematically with lattice constant c , $F_1 = 309$ T, $F_2 = 316$ T, $F_3 = 349$ T. Values for F are determined and cross-checked using fits to Eq. (1), analyses of the fast Fourier transform (FFT) spectra, and Landau level indexing (see Figs. SM2 and SM3 in the Supplemental Material). The Onsager relation $F = (\frac{\hbar}{2\pi e}) A_F$ relates the frequency F to the extremal FS area A_F . We find $A_k = 2.8$ nm $^{-2}$; this is $\approx 1.1\%$ of the Brillouin zone (BZ) volume $A_{BZ} = (2\pi/a)^2 = 252$ nm $^{-2}$ (a is the in-plane lattice constant). This small BZ fraction indicates a reconstructed FS. No other frequencies are visible in either the raw signal (Fig. 3) or in the FFT, including the vicinity of ~ 10 kT (corresponding to $A_F \sim 0.4A_{BZ}$) that would be consistent with a large FS cylinder or magnetic breakdown as observed in NCCO [6].

From the temperature dependence of the QO amplitudes [R_T in Eq. (1)] we extract the quasiparticle effective mass m^* , which can differ from the band mass due to the renormalization of many-body effects. The QO amplitude is plotted versus temperature in Fig. 3(c), along with single-parameter fits to $R(T) = X / \sinh(X)$ with $X \equiv 2\pi^2 k_B T m^* / \hbar e B$ for each sample. The resulting m^* values increase by more than a factor of 2, as $m^* = 1.3 \pm 0.2 m_e$ for sample S1 and $0.55 \pm 0.1 m_e$ for S2, with only slight variation in the tuning parameter c . This strong enhancement of m^* occurs near the crossover between metallic and insulating behavior observed for these

films as a function of c (as discussed later) and suggests proximity to a critical point, tuned by δ as reflected in the value of c .

Charge order, which has been observed widely in both electron- and hole-doped cuprates [4,8,9], is a likely origin for the quantum oscillatory phenomena. Using resonant x-ray scattering [geometry depicted in Fig. 4(a)], we confirm that the same kind of charge order observed in bulk materials also exists in these $\text{Pr}_2\text{CuO}_{4\pm\delta}$ films. To do so, we examine the sample whose largest m^* suggests proximity to an underlying quantum critical point. RXS experiments used x rays tuned to the Cu L_3 edge, greatly enhancing our sensitivity to valence electrons in the CuO_2 planes [Fig. 4(b)]. The distinct peak near $q = (-0.23, 0)$ r.l.u. is suppressed as the photon energy is tuned away from resonance, confirming its electronic origin [Fig. 4(c)]. The peak appears to be weakly temperature dependent up to ~ 275 K, as shown in Figs. 4(d) and 4(e), which is consistent with the observations of similar features in bulk systems. Just as in bulk systems, the onset temperature appears much higher than the pseudogap [9]. Nevertheless, the observation of the $q = (-0.23, 0)$ r.l.u. peak confirms charge order in our thin films, suggesting there is an associated reconstructed Fermi surface.

IV. DISCUSSION

In Fig. 5 we show a comparison of transport properties between our $\text{Pr}_2\text{CuO}_{4\pm\delta}$ thin films and single crystals of $\text{Nd}_{2-x}\text{Ce}_x\text{CuO}_4$ as a function of their c -axis lattice parameter and x , respectively. The low-field Hall numbers [Fig. 5(a)] of $\text{Pr}_2\text{CuO}_{4\pm\delta}$ and $\text{Nd}_{2-x}\text{Ce}_x\text{CuO}_4$ (Ref. [17]) are almost indistinguishable: they show the essential crossover from large, negative to small, positive R_H , indicating a crossover from small to large carrier density near optimal T_c 's. We identify the c -axis lattice constant as a tuning parameter for $\text{Pr}_2\text{CuO}_{4\pm\delta}$, analogous to x in $\text{Nd}_{2-x}\text{Ce}_x\text{CuO}_4$. This analogy is strengthened by noting a similar enhancement in the

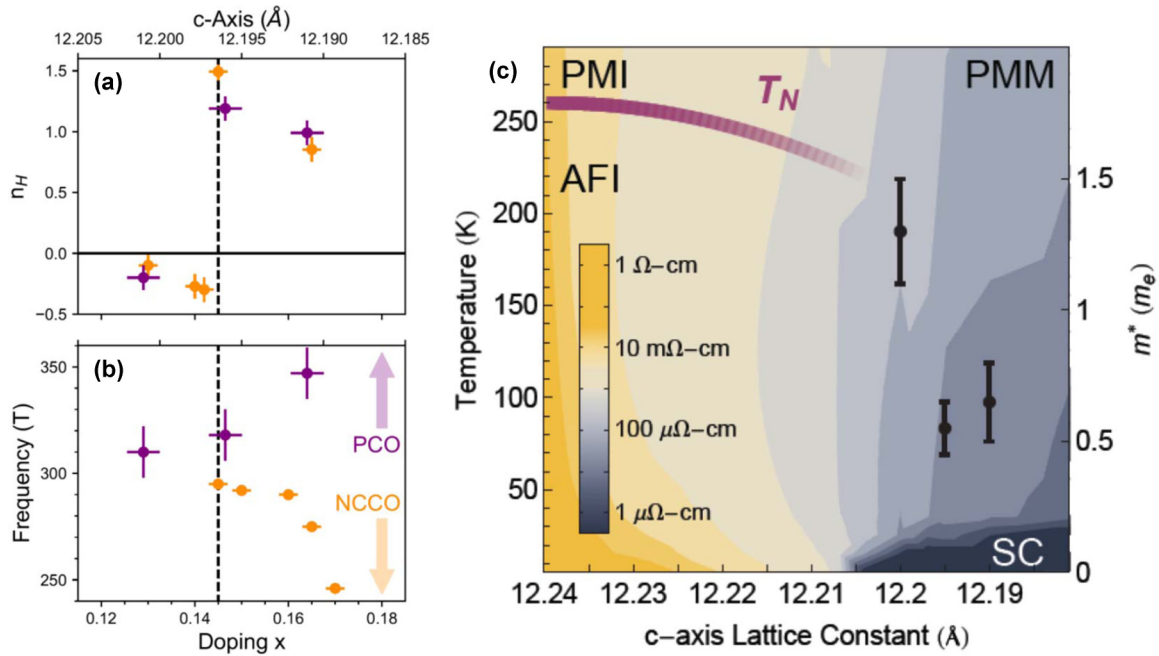


FIG. 5. Universal evolution in $\text{Pr}_2\text{CuO}_{4\pm\delta}$ films. (a) Hall number n_H and (b) QO frequency with c and x for $\text{Pr}_2\text{CuO}_{4\pm\delta}$ films (purple) and $\text{Nd}_{2-x}\text{Ce}_x\text{CuO}_4$ single crystals (orange) (from Ref. [17]). (c) Contour plot of the in-plane resistivity ρ_{xx} as a function of the c -axis lattice parameter and temperature, measured on 18 different $\text{Pr}_2\text{CuO}_{4\pm\delta}$ samples. Also shown (right scale) is the quasiparticle effective mass determined from quantum oscillation measurements (discussed in the text), as well as a schematic boundary (thick line) between the antiferromagnetic insulating phase (AFI) as determined from bulk magnetic measurements of the Néel ordering temperature T_N [30], and the paramagnetic metallic (PMM), insulating (PMI), and superconducting (SC) phases.

effective mass [Fig. 5(c)], and a characteristic “hump” in the magnetoresistance which has been associated with proximity to the QCP [see Fig. 2(c)] [12,27]. These quantum oscillation measurements ostensibly probe the evolution of the FS in this UD-OD crossover region, whereas single-crystal studies have only ever shown this signal on OD materials [6,17,31].

Our experimental results exhibit a crucial difference with the single-crystal studies—the FS area changes by a very small amount, and even appears to *increase* as the critical point is traversed [Fig. 5(b)], whereas in bulk crystals it is observed to decrease [a central argument associating them with holelike pockets arising from a (π, π) reconstruction] [6,17]. Naively, the apparent increase in FS area would suggest that changes in oxygen stoichiometry dope holes in these materials. This would be remarkable (the first hole-doped T' structure reported), but it seems inconsistent with the basic chemistry of the material; there are no chemical dopants, and annealing is known to reduce the amount of oxygen and therefore will have the effect of electron doping, contrary to the suggested scenario.

A more likely scenario is that the structural changes induced by annealing strongly affect the interelectronic correlations, such as those driving the FS reconstruction. In this scenario, weakening the interactions could serve to decrease the gap, and enlarge the reconstructed pocket. This process may be due to the removal of apical oxygen bringing the material closer to its ideal structure, decreasing the lattice size and thereby increasing the bonding overlap by way of “chemical pressure” [32,33]. This mechanism is well understood in organic superconductors, where different systems have the same electron count but due to the complete substitution

of the cation, compress the structure and thus change the ratio of Coulomb to kinetic energy [34–36]. The observed increase in frequency would then be naturally explained—as the system evolves across the QCP, the interactions grow weaker, decreasing the effective mass and the FS folding, and leading to larger hole pockets, just as we observe. Our data makes a clear case that chemical doping and structural effects cannot be disentangled in these materials.

The scenario we describe has implications for understanding the Ce-doped siblings $\text{Pr}_{2-x}\text{Ce}_x\text{CuO}_4$ —these materials will always exhibit multiple effects of doping and structure, both of which affect the correlations driving electronic order in the system. This may answer a long-standing controversy in these materials as to the exact doping value of the quantum critical point [14,37]. Our study illustrates exactly why this value can be so variable depending on annealing conditions—the structural parameters strongly influence the interactions in the system.

This picture may also explain why QOs are seen far from the putative AFM critical point. In light of the current observations of charge order (Fig. 4) [10], together with similar observations in single crystals [9], it seems a charge density wave may be a likely alternative origin, as it is in the hole-doped systems. Whatever the interpretation of the QOs, however, our interpretation of the role of chemical pressure effects is independent of the origin of the FS reconstruction, and the prevailing picture of the T' materials must account for the systematic effect of structure.

As shown in Fig. 5(c) it is possible to construct a phase diagram based entirely on annealed $\text{Pr}_2\text{CuO}_{4\pm\delta}$ samples, which demonstrates a method to cleanly tune these materials from

the UD to the OD region. Despite being controlled by a different parameter, the similarity between this phase diagram and the traditional picture (Fig. 1) provides a complementary insight into what seeds the low-temperature ground state of the T' cuprates. In tracking the electronic correlations across the QCP separating the UD to OD regions, we have shown that there is an interplay of structural and doping effects that determines the shape of the phase diagram, providing a critical piece of the high- T_C puzzle that should inform the design of future superconducting materials.

ACKNOWLEDGMENTS

We thank the scientific and support staff of the Los Alamos National High Magnetic Lab, Pulsed Field Facility

for their technical assistance throughout this project, and also acknowledge illuminating discussions with B. Ramshaw, N. Harrison, R. Greene, and M. Naito. This work was supported by the Laboratory Directed Research and Development Program at Lawrence Berkeley National Laboratory and used resources of the Advanced Light Source of which is a DOE Office of Science User Facility under Contract No. DE-AC02-05CH11231. A portion of this work was performed at the National High Magnetic Field Laboratory, which is supported by the National Science Foundation Cooperative Agreement No. DMR-1157490, the State of Florida, and the US Department of Energy. R.D.M. and K.A.M. acknowledge support from the DOE BES under “Science of 100 tesla” and Z.Z. acknowledges LANL directors funding under LDRD 20120772. We also acknowledge the support of the Gordon and Betty Moore Foundation.

-
- [1] K. Yamada, K. Kurahashi, Y. Endoh, R. J. Birgeneau, and G. Shirane, *J. Phys. Chem. Solids* **60**, 1025 (1999).
- [2] H. Matsui, T. Takahashi, T. Sato, K. Terashima, H. Ding, T. Uefuji, and K. Yamada, *Phys. Rev. B* **75**, 224514 (2007).
- [3] N. P. Armitage, P. Fournier, and R. L. Greene, *Rev. Mod. Phys.* **82**, 2421 (2010).
- [4] S. Gerber, H. Jang, H. Nojiri, S. Matsuzawa, H. Yasumura, D. A. Bonn, R. Liang, W. N. Hardy, Z. Islam, A. Mehta, S. Song, M. Sikorski, D. Stefanescu, Y. Feng, S. A. Kivelson, T. P. Devereaux, Z.-X. Shen, C.-C. Kao, W.-S. Lee, D. Zhu, and J.-S. Lee, *Science* **350**, 949 (2015).
- [5] R. Comin and A. Damascelli, *Annu. Rev. Condens. Matter Phys.* **7**, 369 (2016).
- [6] T. Helm, M. V. Kartsovnik, M. Bartkowiak, N. Bittner, M. Lambacher, A. Erb, J. Wosnitza, and R. Gross, *Phys. Rev. Lett.* **103**, 157002 (2009).
- [7] Y. Li, W. Tabis, Y. Tang, G. Yu, J. Jaroszynski, N. Barišić, and M. Greven, *Sci. Adv.* **5**, eaap7349 (2019).
- [8] E. H. d. S. Neto, P. Aynajian, A. Frano, R. Comin, E. Schierle, E. Weschke, A. Gyenis, J. Wen, J. Schneeloch, Z. Xu, S. Ono, G. Gu, M. L. Tacon, and A. Yazdani, *Science* **343**, 393 (2014).
- [9] E. H. d. S. Neto, B. Yu, M. Minola, R. Sutarto, E. Schierle, F. Boschini, M. Zonno, M. Bluschke, J. Higgins, Y. Li, G. Yu, E. Weschke, F. He, M. L. Tacon, R. L. Greene, M. Greven, G. A. Sawatzky, B. Keimer, and A. Damascelli, *Sci. Adv.* **2**, e1600782 (2016).
- [10] M. Kang, J. Pellicciari, A. Frano, N. Breznay, E. Schierle, E. Weschke, R. Sutarto, F. He, P. Shafer, E. Arenholz, M. Chen, K. Zhang, A. Ruiz, Z. Hao, S. Lewin, J. Analytis, Y. Krockenberger, H. Yamamoto, T. Das, and R. Comin, *Nat. Phys.* **15**, 335 (2019).
- [11] N. P. Breznay, I. M. Hayes, B. J. Ramshaw, R. D. McDonald, Y. Krockenberger, A. Ikeda, H. Irie, H. Yamamoto, and J. G. Analytis, *Phys. Rev. B* **94**, 104514 (2016).
- [12] Y. Dagan, M. M. Qazilbash, C. P. Hill, V. N. Kulkarni, and R. L. Greene, *Phys. Rev. Lett.* **92**, 167001 (2004).
- [13] W. Yu, B. Liang, P. Li, S. Fujino, T. Murakami, I. Takeuchi, and R. L. Greene, *Phys. Rev. B* **75**, 020503(R) (2007).
- [14] S. Li, S. Chi, J. Zhao, H.-H. Wen, M. B. Stone, J. W. Lynn, and P. Dai, *Phys. Rev. B* **78**, 014520 (2008).
- [15] N. P. Butch, K. Jin, K. Kirshenbaum, R. L. Greene, and J. Paglione, *Proc. Natl. Acad. Sci. USA* **109**, 8440 (2012).
- [16] S. Charpentier, G. Roberge, S. Godin-Proulx, X. Béchamp-Laganière, K. D. Truong, P. Fournier, and P. Rauwel, *Phys. Rev. B* **81**, 104509 (2010).
- [17] T. Helm, M. V. Kartsovnik, C. Proust, B. Vignolle, C. Putzke, E. Kampert, I. Sheikin, E.-S. Choi, J. S. Brooks, N. Bittner, W. Biberacher, A. Erb, J. Wosnitza, and R. Gross, *Phys. Rev. B* **92**, 094501 (2015).
- [18] J. S. Higgins, Y. Dagan, M. C. Barr, B. D. Weaver, and R. L. Greene, *Phys. Rev. B* **73**, 104510 (2006).
- [19] A. J. Schultz, J. D. Jorgensen, J. L. Peng, and R. L. Greene, *Phys. Rev. B* **53**, 5157 (1996).
- [20] P. G. Radaelli, J. D. Jorgensen, A. J. Schultz, J. L. Peng, and R. L. Greene, *Phys. Rev. B* **49**, 15322 (1994).
- [21] Y. Krockenberger, H. Irie, O. Matsumoto, K. Yamagami, M. Mitsuhashi, A. Tsukada, M. Naito, and H. Yamamoto, *Sci. Rep.* **3**, 2235 (2013).
- [22] M. Matsuda, Y. Endoh, K. Yamada, H. Kojima, I. Tanaka, R. J. Birgeneau, M. A. Kastner, and G. Shirane, *Phys. Rev. B* **45**, 12548 (1992).
- [23] J. Zhao, P. Dai, S. Li, P. G. Freeman, Y. Onose, and Y. Tokura, *Phys. Rev. Lett.* **99**, 017001 (2007).
- [24] A. Nath, N. S. Kopelev, V. Chechersky, J.-L. Peng, R. L. Greene, B.-h. O, M. I. Larkin, and J. T. Markert, *Science* **265**, 73 (1994).
- [25] See Supplemental Material at <http://link.aps.org/supplemental/10.1103/PhysRevB.100.235111> for additional film characterization and quantum oscillation data and analyses.
- [26] P. Li, F. F. Balakirev, and R. L. Greene, *Phys. Rev. Lett.* **99**, 047003 (2007).
- [27] Y. Dagan, M. C. Barr, W. M. Fisher, R. Beck, T. Dhakal, A. Biswas, and R. L. Greene, *Phys. Rev. Lett.* **94**, 057005 (2005).
- [28] J. S. Higgins, M. K. Chan, T. Sarkar, R. D. McDonald, R. L. Greene, and N. P. Butch, *New J. Phys.* **20**, 043019 (2018).
- [29] D. Shoenberg, *Magnetic Oscillations in Metals*, 1st ed. (Cambridge University Press, Cambridge, 2009).
- [30] M. Matsuda, K. Yamada, K. Kakurai, H. Kadowaki, T. R. Thurston, Y. Endoh, Y. Hidaka, R. J. Birgeneau, M. A. Kastner, P. M. Gehring, A. H. Moudden, and G. Shirane, *Phys. Rev. B* **42**,

- 10098 (1990); D. E. Cox, A. I. Goldman, M. A. Subramanian, J. Gopalakrishnan, and A. W. Sleight, *ibid.* **40**, 6998 (1989); P. Allenspach, S. W. Choeng, A. Dommann, P. Fischer, Z. Fisk, A. Furrer, H. R. Ott, and B. Rupp, *Z. Phys. B* **77**, 185 (1989).
- [31] T. Helm, M. V. Kartsovnik, I. Sheikin, M. Bartkowiak, F. Wolff-Fabris, N. Bittner, W. Biberacher, M. Lambacher, A. Erb, J. Wosnitza, and R. Gross, *Phys. Rev. Lett.* **105**, 247002 (2010).
- [32] M. Suaaidi, J. L. García-Muñoz, S. Piñol, P. Vigoureux, J. Fontcuberta, and X. Obradors, *Physica C (Amsterdam)* **235–240**, 789 (1994).
- [33] J. L. García-Muñoz, M. Suaaidi, J. Fontcuberta, S. Piñol, and X. Obradors, *Physica C (Amsterdam)* **268**, 173 (1996).
- [34] R. H. McKenzie, *Science* **278**, 820 (1997).
- [35] M. Ikeda, T. Yoshida, A. Fujimori, M. Kubota, K. Ono, H. Das, T. Saha-Dasgupta, K. Unozawa, Y. Kaga, T. Sasagawa, and H. Takagi, *Phys. Rev. B* **80**, 014510 (2009).
- [36] B. J. Powell, E. Yusuf, and R. H. McKenzie, *Phys. Rev. B* **80**, 054505 (2009).
- [37] E. M. Motoyama, G. Yu, I. M. Vishik, O. P. Vajk, P. K. Mang, and M. Greven, *Nature (London)* **445**, 186 (2007).